



# A novel method to identify sub-seasonal clustering episodes of extreme precipitation events and their contributions to large accumulation periods

Jérôme Kopp<sup>1</sup>, Pauline Rivoire<sup>1</sup>, S. Mubashshir Ali<sup>1</sup>, Yannick Barton<sup>1</sup>, and Olivia Martius<sup>1</sup>

<sup>1</sup>Oeschger Centre for Climate Change Research and Institute of Geography, University of Bern, Bern, Switzerland

**Correspondence:** Jérôme Kopp (jerome.kopp@giub.unibe.ch)

**Abstract.** Temporal (serial) clustering of extreme precipitation events on sub-seasonal time scales is a type of compound event. It can cause large precipitation accumulations and lead to floods. We present a novel, count-based procedure to identify episodes of sub-seasonal clustering of extreme precipitation. We introduce two metrics to characterise the frequency of sub-seasonal clustering episodes and their relevance for large precipitation accumulations. The procedure does not require the investigated variable (here precipitation) to satisfy any specific statistical properties. Applying this procedure to daily precipitation from the ERA5 reanalysis data set, we identify regions where sub-seasonal clustering occurs frequently and contributes substantially to large precipitation accumulations. The regions are the east and northeast of the Asian continent (north of Yellow Sea, in the Chinese provinces of Hebei, Jilin and Liaoning; North and South Korea; Siberia and east of Mongolia), central Canada and south of California, Afghanistan, Pakistan, the southeast of the Iberian Peninsula, and the north of Argentina and south of Bolivia. Our method is robust with respect to the parameters used to define the extreme events (the percentile threshold and the run length) and the length of the sub-seasonal time window (here 2 – 4 weeks). This procedure could also be used to identify temporal clustering of other variables (e.g. heat waves) and can be applied on different time scales (sub-seasonal to decadal). The code is available at the listed GitHub repository.

## 1 Introduction

Regional-scale extreme precipitation events can affect the entire catchment area of a river or a lake and result in flooding. Floods can have significant socio-economic impacts such as shortages of drinking water, water-borne diseases, and the displacement of people (e.g., IPCC, 2014). The impact of catchment wide precipitation extremes is intensified when the events happen in close temporal succession, i.e., when they are serially clustered. The sub-seasonal serial clustering of extreme precipitation is a temporally compounding event (Zscheischler et al., 2020) and it is relevant for several reasons. First, it can lead to floods in rivers and catchment areas with a high retention capacity. Examples include several floods in Lake Maggiore in Southern Switzerland (Barton et al., 2016), the floods in England in winter 2013/2014 (Priestley et al., 2017), the floods in Pakistan in



2010 (e.g., Lau and Kim, 2012; Martius et al., 2013), and the floods in China in summer 2020 (Guo et al., 2020). Second, the short recovery time between events can overburden rescue and response teams and prevent proper clean-up and efficient repairs to damaged protective structures (Raymond et al., 2020). Third, temporal dependence of precipitation and other extremes is of interest for insurance companies (Priestley et al., 2018) as floods are a major cause of financial loss from natural hazards (European Environment Agency, 2020).

A number of previous studies have analyzed the statistical properties of the serial clustering of extreme events. Mailier et al. (2006); Vitolo et al. (2009), Pinto et al. (2013) and Bevacqua et al. (2020) studied European winter storms (see Dacre and Pinto (2020) for a review), Villarini et al. (2011) quantified clustering of extreme precipitation in the North American Midwest, and Villarini et al. (2012) focused on extreme flooding in Austria. In these studies, clustering in time was assessed using the index of dispersion (variance-to-mean ratio) of a one-dimensional homogeneous Poisson process model i.e., a Poisson process with a constant rate of occurrence (Cox and Isham, 1980). Villarini et al. (2013) analyzed flood occurrence in Iowa using a Cox regression model i.e., a Poisson process with a randomly varying rate of occurrence (e.g., Cox and Isham, 1980; Smith and Karr, 1986). Yang and Villarini (2019) also used a Cox regression model to show that heavy precipitation events over Europe exhibit serial clustering. Their study also indicated that reanalysis products are skillful in reproducing serial clustering identified in observations. Barton et al. (2016) studied serial clustering of extreme precipitation events in southern Switzerland using Ripley's K function (Ripley, 1981) applied to a one-dimensional time axis (Dixon, 2002).

All studies discussed above used statistical models to identify significant serial clustering of extreme events. However, none of those methods are able to directly identify individual clustering episodes. To our knowledge, no procedure exists that (1) automatically identifies individual serial clustering episodes of extreme (precipitation) events, and (2) subsequently uses the identified episodes to evaluate the clustering properties of a region. Here we propose a novel count-based procedure to study serial clustering of catchment-aggregated heavy precipitation using daily precipitation data from ERA5 (Hersbach et al., 2020). We investigate sub-seasonal serial clustering of extreme precipitation events in the mid-latitudes of the Northern and Southern hemisphere. We also quantify the contribution of sub-seasonal serial clustering to large sub-seasonal precipitation accumulations at the catchment level. More specifically, we address the following questions: (1) Globally, what are the regions (catchments) where sub-seasonal serial clustering of extreme precipitation occurs frequently? (2) What is the contribution of sub-seasonal clustering to large sub-seasonal (14 to 28 days) precipitation accumulations? (3) Are the results affected by the choice of the parameters used to identify the extreme events and the length of the period (sensitivity analysis)?

The paper is organised as follows: the data and methods are introduced in section 2. The results are presented and discussed in section 3. Finally, general conclusions and future research avenues are presented in section 4.

## 2 Data and Methods

### 2.1 Catchment selection and precipitation aggregation

This study uses precipitation from the ERA5 reanalysis data set (Hersbach et al., 2020) by the European Centre for Medium-Range Weather Forecasts (ECMWF). The precipitation fields are interpolated to a  $0.25^\circ \times 0.25^\circ$  spatial grid and the hourly

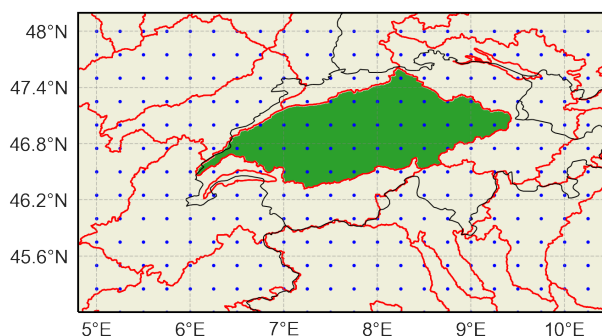


**Figure 1.** Example of a catchment area (Aare basin, Switzerland in green). The red lines show the HydroBASINS level 6 catchment area division. The blue dots indicate the ERA5 grid points. Country borders are indicated by black lines.

precipitation aggregated to daily precipitation for the period 2 January 1979 to 31 March 2019. Precipitation in ERA5 is a prognostic variable.

For catchment boundaries we use the HydroBASINS data set format 2 (with inserted lakes) (Lehner and Grill, 2013). HydroBASINS contains a series of polygon layers that delineate catchment area boundaries at a global scale. This data set has a grid resolution of 15 arc-seconds, corresponding to approximately 500 m at the equator. The HydroBASINS product provides 12 levels of catchment area delineations. The first 3 levels are assigned manually, with level 1 distinguishing 9 continental regions. From Level 4 onward, the breakdown follows a Pfafstetter coding, where a larger basin is sequentially subdivided into 9 smaller units: the 4 largest tributaries and the 5 inter-basins. A basin is divided into two sub-basins at every location where two river branches meet and where they have an individual upstream area of at least 100 km<sup>2</sup>. We use level 6 of HydroBASINS for our study.

Daily precipitation aggregated by catchment area was computed by taking the average of all ERA5 grid points values located within the catchment area (see Fig. 1 for an illustration). Computations were performed using the GeoPandas (version 0.6.0 and onward) Python library (Jordahl et al., 2019). Some small or elongated catchments had few or no grid points inside their boundaries. This is a consequence of the Pfafstetter coding used to construct the HydroBASINS division, where large differences can exist in the catchment areas for a given level. We retained only catchments containing at least five ERA5 grid points for our analyses.

Further, we kept only catchments located in two latitudinal bands between 20° and 70° with a catchment 99<sup>th</sup> annual percentile (99p) of daily precipitation above 10 mm. Those criteria remove catchments from the tropics and the poles, as well as dry areas. The timing of precipitation extremes is important for our analyses and Rivoire et al. (18 January 2021) showed that the timing of extreme precipitation is well captured by ERA5 in the extratropics but less so in the tropics. Figure 2 shows the 99<sup>th</sup> annual percentile of daily precipitation for the 6466 selected catchments.

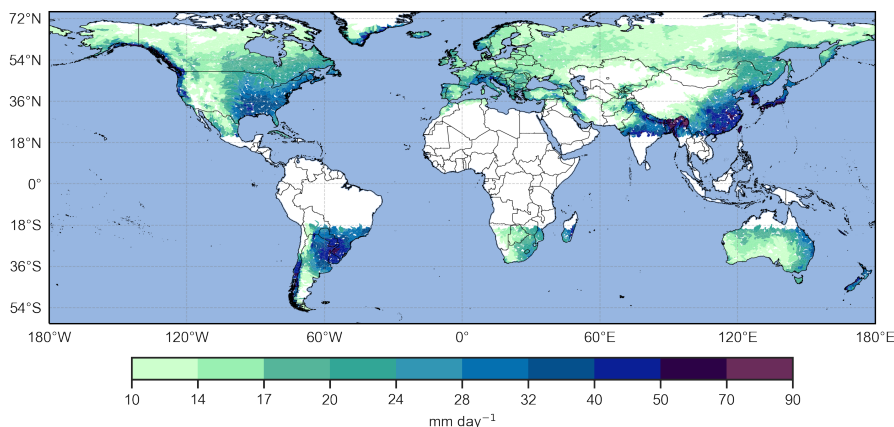


**Figure 2.** The 99<sup>th</sup> annual percentile of daily precipitation per catchment ( $\text{mm day}^{-1}$ ). White areas correspond to the catchments that have been excluded from the analysis.

## 2.2 Identification of extreme precipitation events

We used a Peak-Over-Threshold approach to identify extreme precipitation events from the time series of daily precipitation per catchment (Coles, 2001). We consider only the precipitation values exceeding the local annual 99<sup>th</sup> percentile. We use  
80 annual percentiles rather than seasonal percentiles because they are more impact relevant. To analyse sub-seasonal serial clustering, high frequency clustering had to be removed from the daily precipitation time series. High frequency clustering, i.e. successive days of extreme precipitation, can be caused by a stationary synoptic system (e.g., an extratropical cut-off cyclone). We employed the "runs declustering" method to account for the high frequency clustering (Ferro and Segers, 2003). Thereby, given a run length  $r$  and a threshold  $t$ , days with precipitation exceeding  $t$  that are separated by less than  $r$  days  
85 with precipitation below  $t$  were grouped into one high-frequency cluster (see Fig. 3a for an illustration). After applying the declustering approach, a series of independent extreme daily precipitation events was defined. In the case of a high frequency cluster, the first day of the cluster was retained as the representative day for the event.

The choice of the two parameters ( $t$  and  $r$ ) affects the distribution of independent extreme events (Coles, 2001). We followed the empirical approach of Barton et al. (2016) to determine reasonable values for the parameters. First, we selected two different  
90 thresholds: the 98<sup>th</sup> and 99<sup>th</sup> annual percentiles (further denoted as 98p and 99p) of the catchment area daily precipitation distribution. These thresholds have been used in previous studies (e.g. Fukutome et al., 2015).

The run length can either be determined with an objective method (Barton et al., 2016; Fukutome et al., 2015) or chosen based on meteorological process arguments (Lenggenhager and Martius, 2019). Following the approach of Lenggenhager and Martius (2019), we tested run lengths of both one and two days, corresponding to the influence time of a cyclone at one location  
95 (Lackmann, 2011).

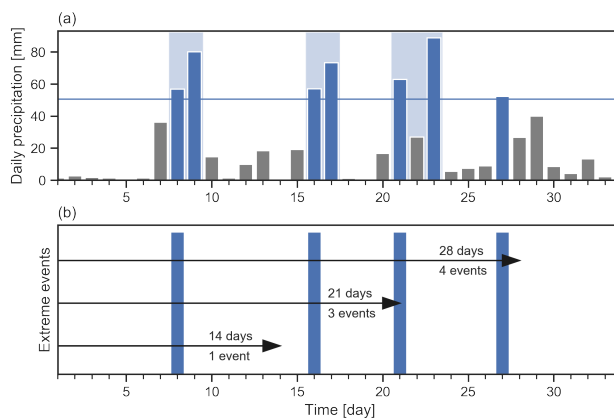


**Figure 3.** (a) Schematic illustration of high-frequency clustering in a time series of daily precipitation with extreme precipitation events marked by blue bars. The horizontal blue line represents a user-defined high precipitation threshold  $t$ . The resulting high-frequency clusters for  $r = 2$  days are highlighted by the light blue shading. (b) Schematic illustration of sub-seasonal clustering: The blue bars indicate the representative days of the extreme precipitation events after the removal of the high-frequency clustering. The number of extreme events contained in time windows starting on day 1 and of various lengths are shown.

The R package `evd` (Stephenson, 2002) was used for the computation of the yearly percentiles and the identification of independent peaks over the threshold, i.e. for the removal of the high-frequency clusters with the runs declustering described above.

### 2.3 Identification of sub-seasonal clustering episodes

100 The following procedure is used to automatically identify sub-seasonal clustering episodes. We start by counting the number of extreme precipitation events ( $n_w$ ) contained in a moving time window of  $w$  days after applying a runs declustering (as illustrated in Fig. 3b). In parallel, we calculate the precipitation accumulation ( $acc_w$ ) for the moving time window.  $n_w$  and  $acc_w$  are computed for each day of the time series over the next  $w - 1$  days (not  $w$ , as the starting day is included in the time window length). Our results are robust to the choice of a centred or lagged time window, except at the boundaries of the series.

105 Time windows of 14, 21 and 28 days are investigated. Figures 4a and 4b reproduce the example of Fig. 3, along with the corresponding values of  $n_w$  (Fig. 4c) and  $acc_w$  (Fig. 4d) for  $w = 14$  days.

We then run our automated clustering episode identification algorithm that consists of the following steps: (i) isolate time windows with the highest count of extreme events  $n_w$ ; (ii) from these, select the time window with the largest precipitation accumulation  $acc_w$ , this is the first clustering episode; (iii) remove all days within  $w - 1$  days before and after the starting day of the first episode from the initial time series, to avoid any overlap between the selected episodes; (iv) repeat steps (ii) and (iii) on the reduced time series, until a pre-determined number  $N_{ep}$  of clustering episodes is identified (the choice of  $N_{ep}$  is discussed further below). This iterative selection results in the identification of non-overlapping clustering episodes sorted in a decreasing order by extreme event counts, and then by precipitation accumulations. We denote this classification as  $Cl_n$ .

110

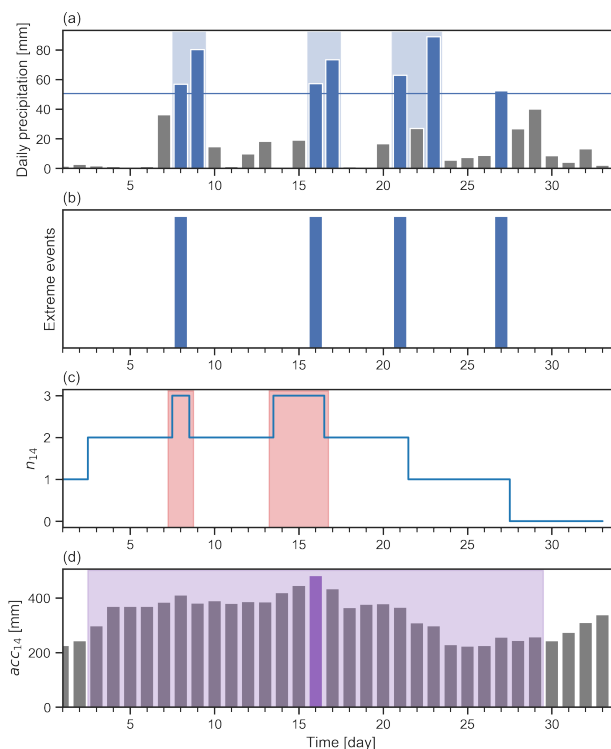


**Figure 4.** Schematic illustration of the identification of sub-seasonal clustering episodes with  $w = 14$  days. Panels (a) and (b) are identical to Fig. 3. (c) Number of extreme precipitation events in the moving time window of 14 days ( $n_{14}$ ) corresponding to the time series in (a); the light red rectangles indicate the days with the highest  $n_{14}$ . (d) Precipitation accumulation in a moving time window of 14 days ( $acc_{14}$ ) corresponding to the time series in (a); the purple bar denotes the day with the largest  $acc_{14}$  among the days with highest  $n_{14}$ . This day is therefore defined as the starting day of the first selected episode in both classifications  $Cl_n$  and  $Cl_{acc}$ , and all days within the light purple rectangle are removed from the initial time series.

In addition, we identify and classify episodes with high to extreme precipitation accumulation, denoted as  $Cl_{acc}$ . This is done  
 115 by applying steps (ii) to (iv) of our automated identification algorithm to the original precipitation time series. The episodes  
 picked out by the clustering episode identification and the extreme precipitation accumulation identification can be partly or  
 completely identical. Examples of  $Cl_n$  and  $Cl_{acc}$  for the time series of Fig. 4 are shown in Table 1. Sub-seasonal clustering  
 frequency and contribution to large accumulations can now be assessed based on the two classifications.

## 120 2.4 Metrics for sub-seasonal clustering

As a preliminary remark, we note that if the  $Cl_n$  classification of a given catchment has many clustering episodes that contain  
 several extreme events, then sub-seasonal clustering is occurring frequently in that catchment. Similarly, if the two classifica-



**Table 1.** Sub-seasonal clustering episodes corresponding to Fig. 4 and their respective rank in the  $Cl_n$  and  $Cl_{acc}$  classifications. The columns  $Cl_n$  and  $Cl_{acc}$  are empty for episodes excluded from the classifications. For this example,  $S_f = \sum_{i \in Cl_n} n_w(i) \cdot q_i = 3 \cdot 1 + 1 \cdot 0.38 + 0 \cdot 0.16 = 3.38$ ,  $S' = \sum_{i \in Cl_{acc}} n_w(i) \cdot q_i = 3 \cdot 1 + 0 \cdot 0.38 + 1 \cdot 0.16 = 3.16$  and  $S_r = \frac{S'_f}{S_f} = \frac{3.16}{3.38} = 0.93$  (see section 2.4 for the definitions of  $S_f$  and  $S_r$ ).

Starting day	$n_{14}$	$acc_{14}$ [mm]	Rank $Cl_n$	Rank $Cl_{acc}$
<b>16</b>	<b>3</b>	<b>482.44</b>	<b>1</b>	<b>1</b>
8	3	411.04		
17	2	433.90		
10	2	389.96		
7	2	384.41		
22	1	309.08		
<b>2</b>	<b>1</b>	<b>243.92</b>	<b>2</b>	<b>3</b>
<b>33</b>	<b>0</b>	<b>339.28</b>	<b>3</b>	<b>2</b>

tions  $Cl_n$  and  $Cl_{acc}$  have episodes with the same number of extreme events at identical ranks, this implies that the episodes with the largest number of extreme events correspond to the episodes with the largest precipitation accumulations. In this case, the contribution of sub-seasonal clustering to large precipitation accumulations is maximised. We would like to build metrics that synthesize the properties of the two classifications and allow us to directly compare catchments. This problem is equivalent to defining a scoring system, where each episode is given a weight  $q_i$  depending on its position in the classification, and by taking into account the number of extreme events in each episode. We will use the method of the incenter of a convex cone following (Sitarz, 2013) to construct our weighting scheme. Sitarz (2013) assume two intuitive conditions for a scoring system. First, they assign more points for the first place than for the second place, and more for the second than for the third, and so on. Second, the difference between the  $i^{th}$  place and the  $(i+1)^{th}$  place should be larger than the difference between the  $(i+1)^{th}$  place and the  $(i+2)^{th}$  place. This is equivalent to considering the following set of points:

$$K = \{(x_1, x_2, \dots, x_N) \in \mathbb{R}^N : x_1 \geq x_2 \geq \dots \geq x_n \geq 0 \text{ and } x_1 - x_2 \geq x_2 - x_3 \geq \dots \geq x_{N-1} - x_N\} \quad (1)$$

where  $x_1$  denotes the points for the first place,  $x_2$  the points for the second place, ..., and  $x_N$  the points for the  $N^{th}$  place. Any choice of points in  $K$  would satisfy the two conditions for a scoring system, however we would like to have a unique and representative value. The option chosen by Sitarz (2013) is to look for the equivalent of a mean value: the incenter of  $K$ . Formally, the incenter is defined as an optimal solution of the following optimization problem by Henrion and Seeger (2010):

$$\max_{x \in K \cap S_x} dist(x, \partial K) \quad (2)$$

where  $S_x$  denotes the unit sphere,  $\partial K$  denotes the boundary of set  $K$  and  $dist$  denotes the distance in the Euclidean space. By using the calculation presented in the Appendix of Sitarz (2013), and dividing by the parameter  $\lambda$  and the points of the first



place ( $\bar{x}_1$ ) to get the weights ( $q_i$ ), we obtain:

$$q_N = \frac{1}{\bar{x}_N}$$

$$q_{N-1} = \frac{\sqrt{2} + 1}{\bar{x}_N}$$

$$q_{N-2} = \frac{(\sqrt{2} + 1)(\sqrt{3} + 2) - (\sqrt{3} + 1)}{\bar{x}_N}$$

145 ...

$$q_i = \frac{3\bar{x}_{i-1} - 3\bar{x}_{i-2} + \bar{x}_{i-3}}{\bar{x}_N}, \text{ for } i = N - 3, \dots, 2$$

...

$$q_1 = 1$$

The weight  $q_1$  is always 1 but the values of weights  $q_2$  to  $q_N$  depend on  $N$  and in our case  $N$  is the number of clustering episodes  
 150  $N_{ep}$ . The first metric  $S_f$  that describes the propensity of a catchment for sub-seasonal clustering is defined as the product of  
 the weight  $q_i$  by the corresponding number of extreme events in the  $i^{th}$  episode  $n_w(i)$  summed over all  $N_{ep}$  episodes in the  
 $Cl_n$  classification (Eq. (3)):

$$S_f = \sum_{i \in Cl_n} n_w(i) \cdot q_i \quad (3)$$

We refer to  $S_f$  as the frequency metric, since it measures how often sub-seasonal clustering episodes happen and how many  
 155 extreme events these episodes contain. High values of  $S_f$  imply that the first  $N_{ep}$  sub-seasonal clustering episodes contain a  
 large number of extreme events.

The second metric  $S_r$  describes how sub-seasonal clustering episodes contribute to large sub-seasonal precipitation accumula-  
 tions. It is defined as the ratio of  $S'_f$  to  $S_f$ , where  $S'_f$  is computed the same way as  $S_f$ , but this time using the  $Cl_{acc}$  classification  
 (Eq. (4)):

$$160 \quad S_r = \frac{S'_f}{S_f} \quad \text{with} \quad S'_f = \sum_{i \in Cl_{acc}} n_w(i) \cdot q_i \quad (4)$$

We refer to  $S_r$  as the relevance metric.  $S_r$  is unit-less. It ranges between 0 and 1 and measures the degree of similarity between  
 the two classifications.  $S_r$  is equal to 1 when  $S'_f = S_f$ , i.e. when the two classifications have episodes with the same number  
 of extreme events at identical ranks. The episodes may not be classified in the exact same order, however, they are ranked  
 by their respective  $n_w$  in a strict descending order in both classifications.  $S_r$  equal to 0 implies that the  $N_{ep}$  episodes in  
 165 the  $S'_f$  classification contain no extreme events ( $n_w(i) = 0 \forall i \in [1, N_{ep}]$ ). Thus, the episodes with the largest precipitation  
 accumulations contain no extreme events. In the example of Tab. 1,  $S_r$  is close to 1, hence sub-seasonal clustering episodes  
 contribute substantially to the three top 14-day precipitation accumulations.

The exact interpretation of intermediary values of  $S_r$  requires to look at both classifications ( $Cl_n$  and  $Cl_{acc}$ ) in detail to see  
 where they differ from each other. For example,  $S_r = 0.8$  means that both classifications have a high degree of similarity and





170 that sub-seasonal clustering episodes contribute to large precipitation accumulations. However, it does not imply that 80% of  
the episodes have ranked equally in both classifications. The fact that  $S_r$  is normalised allows to compare different catchments  
and assess their sensitivity to the choice of the parameters. Note that performing a regression between  $Cl_n$  and  $Cl_{acc}$  would  
require to give a unique identifier to each episode according to its starting day. In that case, the strength of the regression would  
be lowered when two episodes containing the same number of extreme events just swap their ranks in the two classifications.  
175 Such a change does not affect  $S_r$ . Hence a regression would be a more conservative approach in assessing the contribution of  
clustering episodes to accumulations.

Both scores depend on the number of clustering episodes considered ( $N_{ep}$ ). The choice of  $N_{ep}$  is arbitrary but should be  
guided by some principles. The same value of  $N_{ep}$  should be chosen for both  $S_f$  and  $S'_f$  and for all catchments to allow for  
comparisons. This implies that one cannot simply iterate over the precipitation time series until all non-overlapping episodes  
180 have been selected and classified. By doing so, one could end up with different values of  $N_{ep}$  for each catchment. Moreover,  
the contribution of the  $i^{th}$  term to the sums in  $S_f$  and  $S_r$  becomes smaller as  $N_{ep}$  increases. We have tested several values of  
 $N_{ep}$  ranging from 10 to 50 and found that the results with  $N_{ep}$  ranging from 30 to 50 are comparable. Hence, we selected  $N_{ep}$   
= 50 for our analysis.

## 2.5 Correlations with index of dispersion and significance test

185 We computed the index of dispersion  $\phi$  for each catchment (Cox and Isham, 1980; Mailier et al., 2006) to compare our results  
to a more traditional method. For an homogeneous Poisson process,  $\phi = 1$ . When  $\phi > 1$ , the process is more clustered than  
random. When  $\phi < 1$ , the process is more regular than random (Mailier et al., 2006). To estimate  $\phi$  for a given catchment,  
we separated the precipitation time series in successive intervals of  $w$  days and counted the number of extreme events in each  
interval. An estimator of  $\phi$  is then given by (Mailier et al., 2006):

$$190 \quad \hat{\phi} = \frac{s_n^2}{\bar{n}} \quad (5)$$

where  $\bar{n}$  is the sample mean and  $s_n^2$  the sample variance of the number of extreme events in the  $\frac{14199}{w}$  intervals, where 14199  
is the number of days in our time series.

We computed  $S_f$  and  $\hat{\phi}$ , and calculated their Spearman rank correlation coefficient (Wilks, 2011) for all catchments and  
for each parameter combination (Table 2). All correlation coefficients are positive with values between 0.738 and 0.885, and  
195 significant with p-values  $< 10^{-5}$ . Figure 5 displays a scatter plot of  $S_f$  versus  $\hat{\phi}$  for all catchments for the initial parameter  
combination ( $r = 2$  days,  $t = 99p$ ,  $w = 21$  days) and illustrates this correlation. This significant positive correlation means that  
the use of  $S_f$  and  $\hat{\phi}$  lead to similar conclusions about the clustering of extreme precipitation events. This is illustrated in Fig. 6,  
which shows  $S_f$  and  $\hat{\phi}$  for the initial parameter combination and where it can be seen that regions of high (low)  $S_f$  correspond  
to regions of high (low)  $\hat{\phi}$ . Figure 6a is further discussed in the results section.



**Table 2.** Spearman rank correlation coefficients between  $S_f$  and  $\hat{\phi}$  for all parameter combinations.

$r$ [days]	$t$ [p]	$w$ [days]	Cor. coeff.
1	98	14	0.832
1	98	21	0.871
1	98	28	0.885
1	99	14	0.814
1	99	21	0.844
1	99	28	0.860
2	98	14	0.738
2	98	21	0.816
2	98	28	0.840
2	99	14	0.765
2	99	21	0.816
2	99	28	0.836

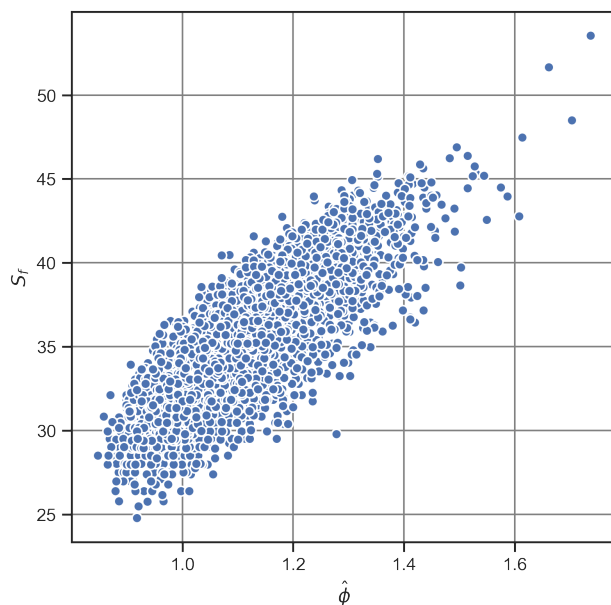


**Figure 5.** Scatterplot of the index of dispersion  $\hat{\phi}$  versus the  $S_f$  metric for all selected catchments for the initial parameter combination ( $r = 2$  days,  $t = 99p$ ,  $w = 21$  days).

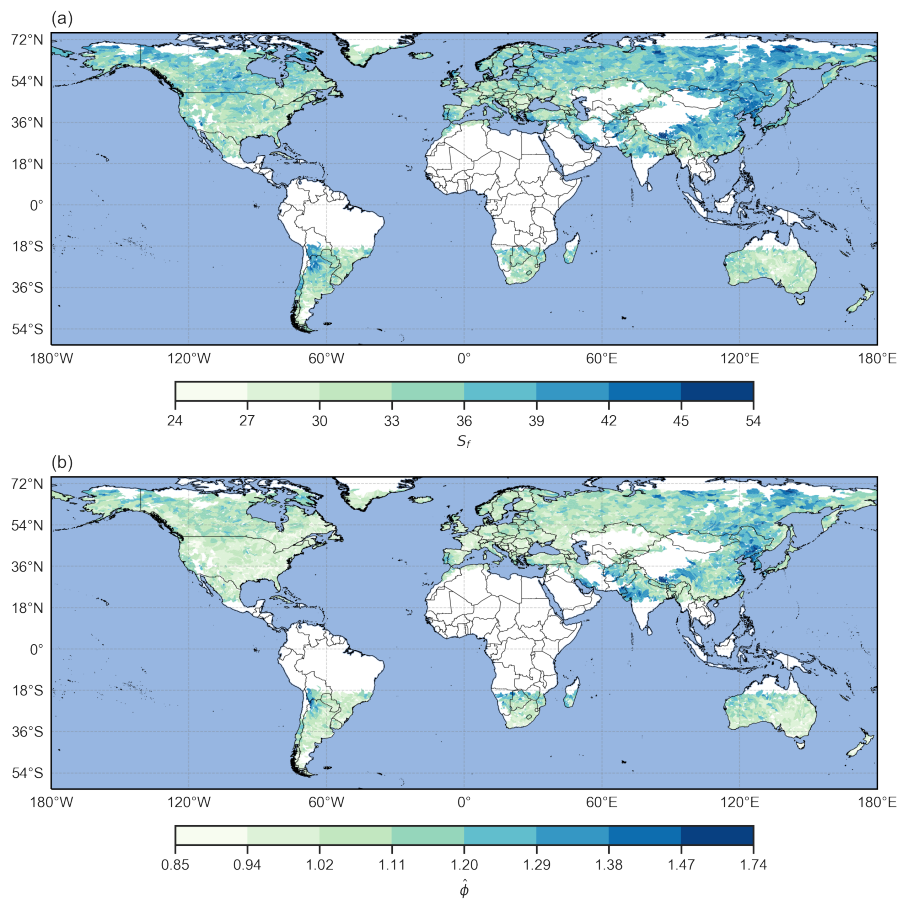


**Figure 6.** Metric  $S_f$  (a) and index of dispersion  $\hat{\phi}$  (b) by catchment, for  $r = 2$  days,  $t = 99p$ ,  $w = 21$  days. In (a), high values of  $S_f$  denote catchments where sub-seasonal clustering occurs frequently. In (b),  $\hat{\phi} > 1$  denote catchments where extreme precipitation events are more clustered than random.



**Table 3.** Symbols for important quantities used in this study.

Symbol	Definition
$r$	Run length parameter (minimal distance between two high-frequency clusters)
$t$	Threshold (above which daily precipitation is considered as an extreme event)
$w$	Time window length (duration of a sub-seasonal clustering episode)
$n_w$	Count of extreme events during a time window of $w$ days
$acc_w$	Precipitation accumulation during a time window of $w$ days
$N_{ep}$	Number of sub-seasonal clustering episodes considered in the classifications
$Cl_n$	Classification of sub-seasonal clustering episodes with the highest extreme event counts, and the largest precipitation accumulations
$Cl_{acc}$	Classification of sub-seasonal clustering episodes with the largest precipitation accumulations
$q_i$	Weight of the $i^{th}$ episode in a classification
$S_f$	Frequency metric
$S_r$	Relevance metric
$\hat{\phi}$	Estimator of the index of dispersion

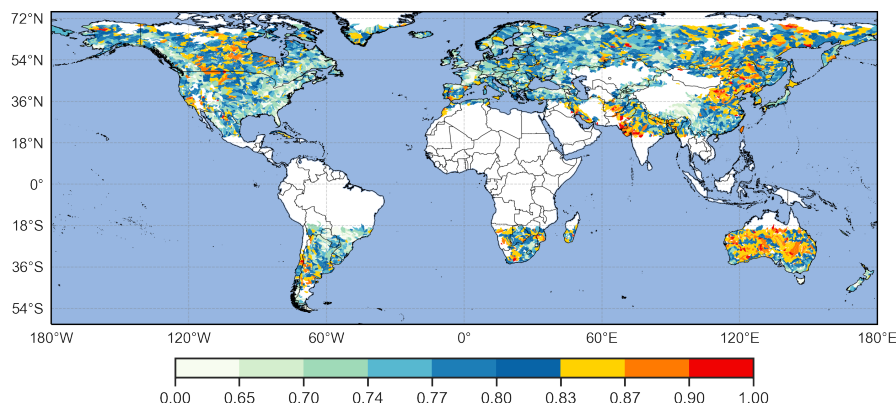


**Figure 7.** Metric  $S_r$  by catchment, for  $r = 2$  days,  $t = 99p$ ,  $w = 21$  days. Values of  $S_r$  close to 1 denote catchments where sub-seasonal clustering contributes substantially to large precipitation accumulations.

## 200 3 Results

First, world maps of the frequency and relevance metrics for all selected catchments are shown using the initial combination of parameters ( $r = 2$  days,  $t = 99p$ ,  $w = 21$  days). These maps indicate regions where sub-seasonal clustering is prevalent. Then, the sensitivity of the sub-seasonal clustering to the parameter choice is assessed by testing 12 different parameter combinations:  $w = 14, 21, 28$  days;  $u = 98p, 99p$ ;  $r = 1, 2$  days.

### 205 3.1 Frequency and precipitation accumulation contributions of sub-seasonal clustering episodes

Catchments with a high frequency metric ( $S_f$ ) (Fig. 6a) are located in the east and northeast of the Asian continent (northeast of Siberia, northeast of China, Korean Peninsula, south of Tibet); between the northwest of Argentina and the southwest of Bolivia; in the northeast and northwest of Canada as well as in Alaska; and in the southwestern part of the Iberian Peninsula. Regions with low values of the frequency metric are located on the east coast of North America, on the east coast of Brazil, 210 in central Europe, in South Africa, in central Australia, in New Zealand and in the north of Myanmar. Catchments with strongly contrasting values of  $S_f$  are rarely found in close proximity, except for a group of catchments located northeast of the Himalayas (south of Tibet), and another group located southeast of the Himalayas (Bangladesh and Myanmar). The catchments to the north have high values of  $S_f$ , whereas the neighbouring catchments to the south exhibit low values of  $S_f$ .

Regions with large values of the relevance metric ( $S_r$ , see Fig. 7) are in the east and northeast of the Asian continent, west of 215 India, central Australia and central North America. Areas with low values of  $S_r$  are located in central China, on the east coast of North America, in the south of Brazil and in France.

Catchments where both  $S_f$  and  $S_r$  have high values are of special interest, because in these catchments sub-seasonal clustering episodes frequently contain multiple extreme events and contribute substantially to large 21-days precipitation accumulations. We highlight catchments where both  $S_f$  and  $S_r$  are high by marking all catchments where  $S_f$  and  $S_r$  are above



220 their respective 75<sup>th</sup> percentile. The choice of the 75<sup>th</sup> percentile is somewhat arbitrary. The results are shown in Fig. 8a. The  
east and northeast of the Asian continent exhibit the largest concentration of catchments where clustering episodes are both  
frequent and contribute to large accumulations. The largest continuous area of such catchments is located north of the Yellow  
Sea, in the Chinese provinces of Hebei, Jilin and Liaoning, in North and South Korea, Siberia and east of Mongolia. Other  
areas with several catchments of interest are central Canada and south California, Afghanistan, Pakistan, the southeast of the  
225 Iberian Peninsula, the north of Argentina and the south of Bolivia. Small groups of two to three or isolated catchments can be  
found on every continent.

We also identify regions with values of  $S_f$  below the 25<sup>th</sup> percentile and values of  $S_r$  above the 75<sup>th</sup> percentile (Fig.  
8b). The low values of  $S_f$  mean that the clustering episodes identified by our algorithm contain a small number or even no  
extreme events, and high values of  $S_r$  mean that those episodes lead to the largest accumulations. Such regions that exhibit  
230 rare clustering, and where this rare clustering contributes substantially to large accumulations are the following: Taiwan, most  
of Australia, central Argentina, South Africa, south of Botswana and south of Greenland. Again, small groups of two to three  
or isolated catchments can be found on every continent. Interestingly, the identified catchments are almost all located in the  
Southern hemisphere.

Finally, we identify regions with values of  $S_f$  above the 75<sup>th</sup> percentile and values of  $S_r$  below the 25<sup>th</sup> percentile (Fig. 8c).  
235 The high values of  $S_f$  mean that the clustering episodes identified by our algorithm contain a relatively large number of extreme  
events, whereas the low values of  $S_r$  mean that episodes leading to the largest accumulations contain a low number or even no  
extreme events. Such regions that exhibit frequent clustering, but where this frequent clustering has a limited contribution to  
large accumulations are the following: the south of Tibet, the south of the Qinghai and west of the Sichuan Chinese provinces  
and central Bolivia. Again, small groups of two to three or isolated catchments can be found on every continent. Only a few  
240 catchments exhibit this combination of high  $S_f$  and low  $S_r$  values, highlighting the importance of the clustering of extreme  
events for generating the largest accumulations for the majority of the catchments.

### 3.2 Sensitivity analysis of $S_r$

The choice of the parameters will affect  $S_f$  for a given catchment. A decrease in the threshold  $t$  and a decrease in the run  
length  $r$  both increase the number of extreme events per episode. An increase in the time window  $w$  increases the likelihood of  
245 capturing more extreme events in a single episode. Together, those changes are expected to increase  $S_f$  for most catchments.  
However, the variations of  $S_r$  with the parameters depends on the variations of both  $S_f$  and  $S'_f$ . If the variations of  $S_f$  and  $S'_f$   
are of the same order of magnitude, then  $S_r$  will change only slightly. It is therefore of interest to perform a sensitivity analysis  
on  $S_r$  by modifying the parameters used to define the clustering episodes to see if the distribution of  $S_r$  remains similar.

Figure 9a shows the distributions of  $S_r$  for all parameters combinations, while Figure 9b displays the distributions of the  
250 difference between the initial parameter combination ( $r = 2$  days,  $t = 99p$ ,  $w = 21$  days) and the other combinations. The data  
used to draw the boxplots can be found in tables A1 and A2 in the appendix. The median value of  $S_r$ , indicated by the  
green lines in the boxplots, exhibits very low sensitivity to changes in the parameters with a minimum value of 0.79 (for  
 $r = 2$  days,  $t = 98p$ ,  $w = 14$  days, see Fig. 9a) and a maximum value of 0.84 ( $r = 1$  days,  $t = 98p$ ,  $w = 28$  days). The same

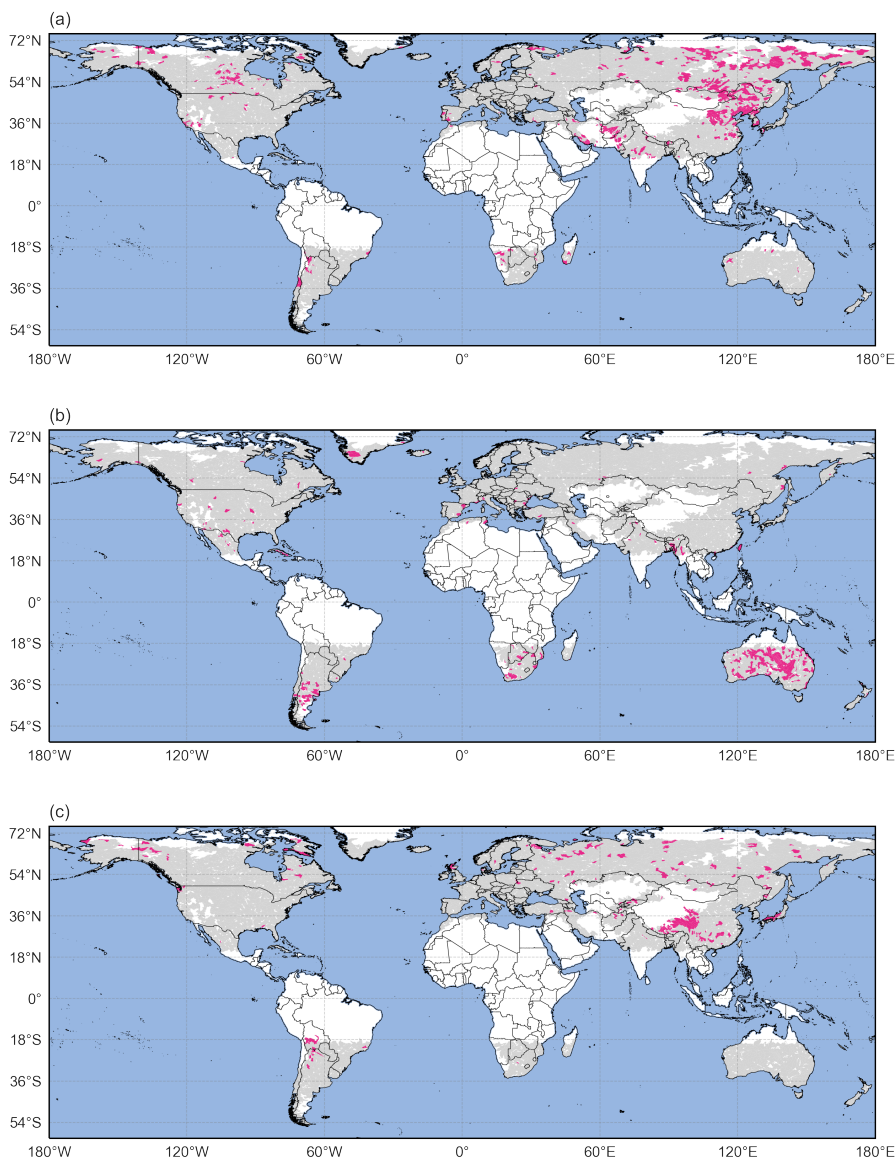


**Figure 8.** (a) Catchments where  $S_f$  and  $S_r$  are both above their respective 75<sup>th</sup> percentile (pink areas); (b) Catchments where  $S_f < 25p$  and  $S_r > 75p$  (pink areas) and (c) Catchments where  $S_f < 75p$  and  $S_r > 25p$  (pink areas). In all panels, catchments in grey do not satisfy the respective conditions, whereas catchments in white were excluded from the analysis according to the criteria defined in section 2.1.

conclusion holds for the mean. In addition, the interquartile range and the position of the outliers are similar for all parameters combinations.

Examination of Fig. 9b reveals that the differences in  $S_f$  and  $S_r$  between the initial combination of parameters and the other combinations are relatively small for most catchments. For example, a change in  $r$  from 2 days to 1 day, while keeping  $t$  and  $w$

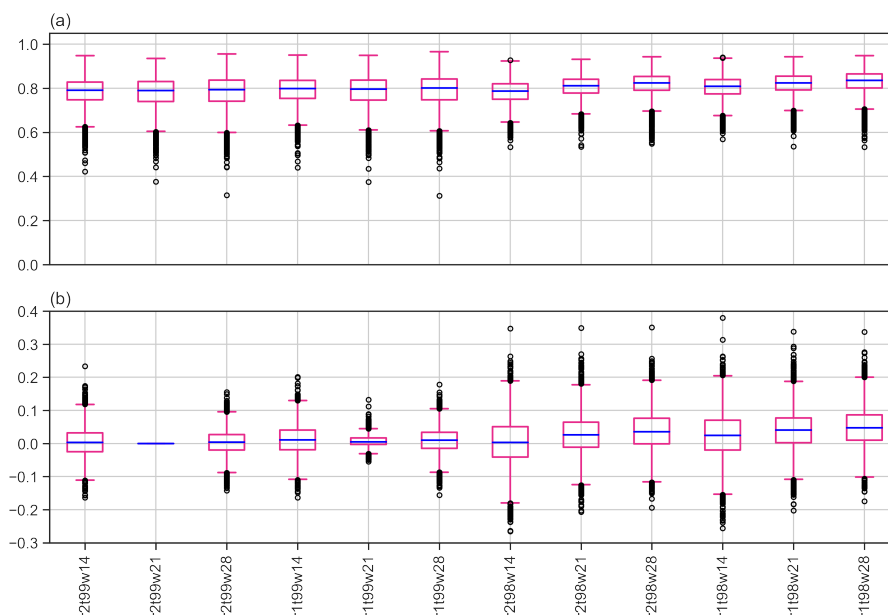


**Figure 9.** Boxplots of (a)  $S_r$  for all catchments and parameters combinations and (b) of the differences in  $S_r$  between the initial parameter combination (the second boxplot from the left, i.e.  $r = 2$  days,  $t = 99p$ ,  $w = 21$  days) and the other combinations. Boxes extend from the first (Q1) to the third (Q3) quartile values of the data, with a blue line at the median. The position of the whiskers is  $1.5 * (Q3 - Q1)$  from the edges of the box. Outlier points past the end of the whiskers are shown with black circles.

constant ( $r = 1$  days,  $t = 99p$ ,  $w = 21$  days), results in an absolute difference in  $S_r$  smaller than 0.05 for almost all catchments. However, the variation can be more substantial for other parameter combinations. For example, a change in  $t$  from  $99p$  to  $98p$  and in  $w$  from 21 to 14 days, while keeping  $r$  constant (e.g.  $r = 2$  days,  $t = 98p$ ,  $w = 14$  days), leads to much larger absolute differences in  $S_r$  that can reach up to 0.35. Moreover,  $S_r$  at a given catchment can exhibit a wide range of variations when looking at all parameters combinations (not shown).

Taking into account the potential for high sensitivity to the parameters, we counted the number of parameter combinations where catchments are above the  $75^{th}$  percentile of both the  $S_f$  and  $S_r$  distributions to reach more robust conclusions. Areas with high counts, i.e. where catchments have been selected in several parameter combinations, are almost identical to the ones identified with the initial parameter combination (Fig. 10a). This means that the parameters selection does not have a substantial impact on the identified regions where sub-seasonal clustering occurs frequently and contributes substantially to large accumulations. This robustness with respect to variations in the parameters is also found for the catchments with  $S_f < 25p$  and  $S_r > 75p$  (rare clustering with substantial contribution), and  $S_f < 75p$  and  $S_r > 25p$  (frequent clustering with limited contribution),



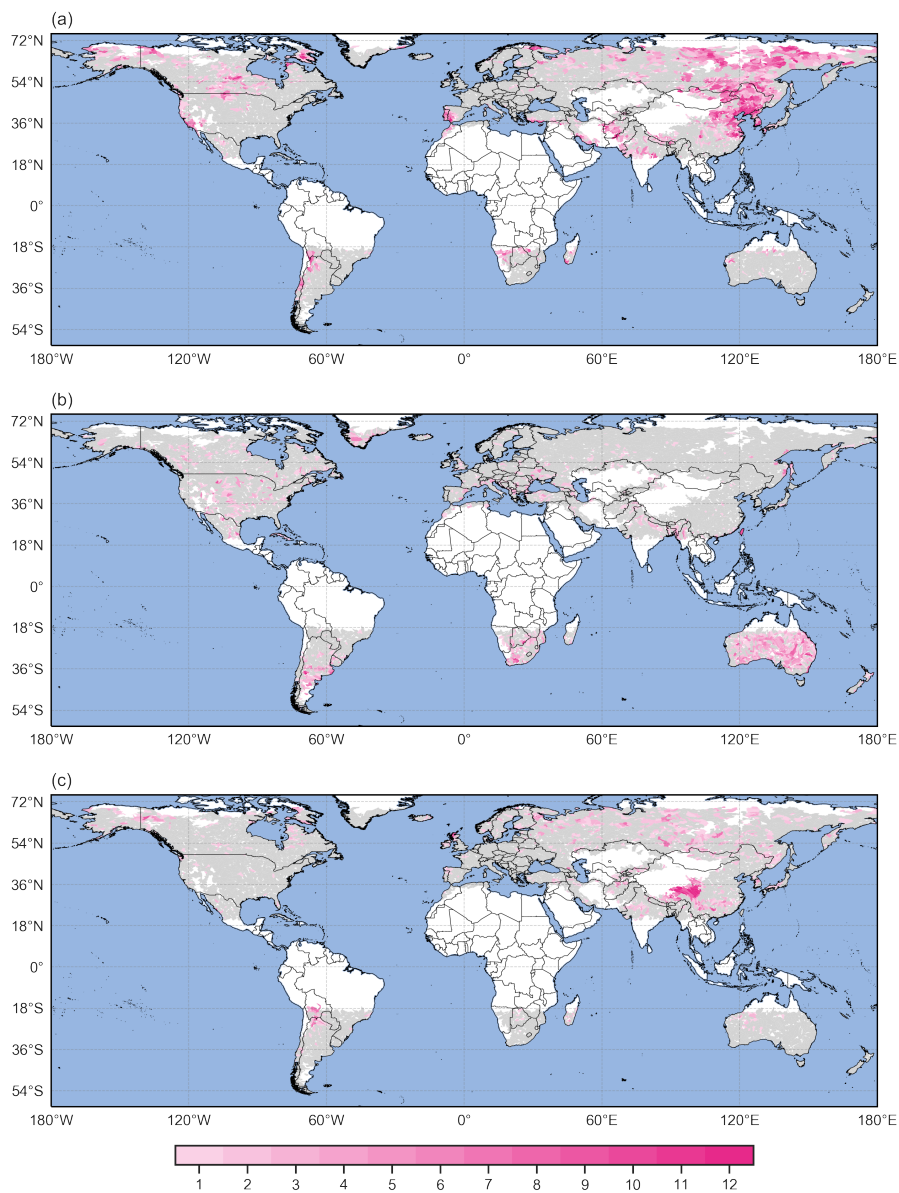


**Figure 10.** (a) Count of parameters combinations where  $S_f > 75p$  and  $S_r > 75p$  (pink areas); (b) Count of parameters combinations where  $S_f < 25p$  and  $S_r > 75p$  (pink areas) and (c) Count of parameters combinations where  $S_f < 75p$  and  $S_r > 25p$  (pink areas). In all panels, catchments in grey do not satisfy the respective conditions for any parameter combination, whereas catchments in white were excluded from the analysis according to the criteria defined in section 2.1.



#### 4 Discussion and conclusions

We present a novel count-based procedure to analyse sub-seasonal clustering of extreme precipitation events. The procedure identifies individual clustering episodes and introduces two metrics to characterise the frequency of sub-seasonal clustering episodes ( $S_f$ ) and their relevance for large precipitation accumulations ( $S_r$ ). The procedure is an avowedly simple count-  
275 based approach that has its advantages and drawbacks. Conceptually, our approach differs from previously proposed methods to quantify sub-seasonal clustering that are based on parametric distributions with associated assumptions on the underlying distributions of the data. A major advantage of our method is that it does not require the investigated variable (here precipitation) to satisfy any specific statistical properties. This allowed us to study annual percentiles, which in most catchments exhibit a strong seasonal cycle. The seasonal cycle violates the independence assumptions underlying the parametric approaches. The  
280 seasonality issue is countered in the parametric approaches by either focusing on a single season (e.g., Mailier et al., 2006) or by including a seasonally varying occurrence rate in the models (Villarini et al., 2013). Working with annual percentiles allows us to focus on high-impact events. This comes at the cost of not being able to distinguish seasonal drivers from other drivers of sub-seasonal clustering. If precipitation in some regions occurs more often or with more intensity during a specific period of the year, then the use of an annual thresholds will result in a more frequent detection of extremes during this specific  
285 period. Consequently, extremes will also be more likely to happen successively in a sub-seasonal time window. Hence, a catchment exhibiting a strong seasonality of extreme precipitation would likely show higher values of  $S_f$  than a catchment where precipitation shows no or weak seasonality.

One shortcoming of our method is the lack of a simple assessment of the significance of the clustering. In mitigation, we note that this can be done using the established methods and that our procedure introduces valuable practical refinements to  
290 the established methods. First, the identification of individual clustering episodes allows researchers to study the atmospheric conditions that prevailed before and during an episode and hence the processes leading to clustering. An illustration is given in Figure 11a, which shows a 21-days clustering episode identified with our procedure for a catchment of the Iberian Peninsula (HydroBASINS ID n° 2060654920), with the corresponding Potential Vorticity and Integrated Vapor Transport composites (Fig. 11b and Fig. 11c, respectively). Second, knowing when clustering episodes happen enables researchers to study their  
295 medium-range to seasonal predictability (see Webster et al. (2011) for an example). Third, the episode identification makes possible to link the precipitation clustering to hydrological impacts (e.g., using disasters data bases or hydrological models). And finally, the  $S_r$  metric allows to globally assess the contribution of sub-seasonal clustering to high precipitation accumulations, which to our knowledge cannot be done with any existing method.

Applying this methodology to the recent ERA5 data set, we identify regions where sub-seasonal clustering of annual high  
300 precipitation percentiles occurs frequently and contributes substantially to large precipitation accumulations. Those regions are the east and northeast of the Asian continent (north of Yellow Sea, in the Chinese provinces of Hebei, Jilin and Liaoning, in North and South Korea, Siberia and east of Mongolia), the central Canada and south of California, Afghanistan, Pakistan, the southeast of the Iberian Peninsula, and the north of Argentina and south of Bolivia. The method is robust with respect to



changes in the parameters used to define the extreme events (the threshold  $t$  and the run length  $r$ ) and the length of the episode  
305 (the time window  $w$ ).

Regions that exhibit frequent clustering according to our approach could be studied with other methods to see if the sub-  
seasonal clustering is due to seasonal effects such as monsoon circulations, changes in sea surface temperatures or seasonal  
variability of the extratropical stormtracks. We also think that our approach is very flexible and that it could also be used to  
identify serial clustering of other variables (e.g. heat waves) and can be applied on different time scales (e.g. for drought years).  
310 An example would be the classification of hurricane seasons using frequency and categories of hurricanes. For this reason, we  
have made our code available on the listed GitHub repository.

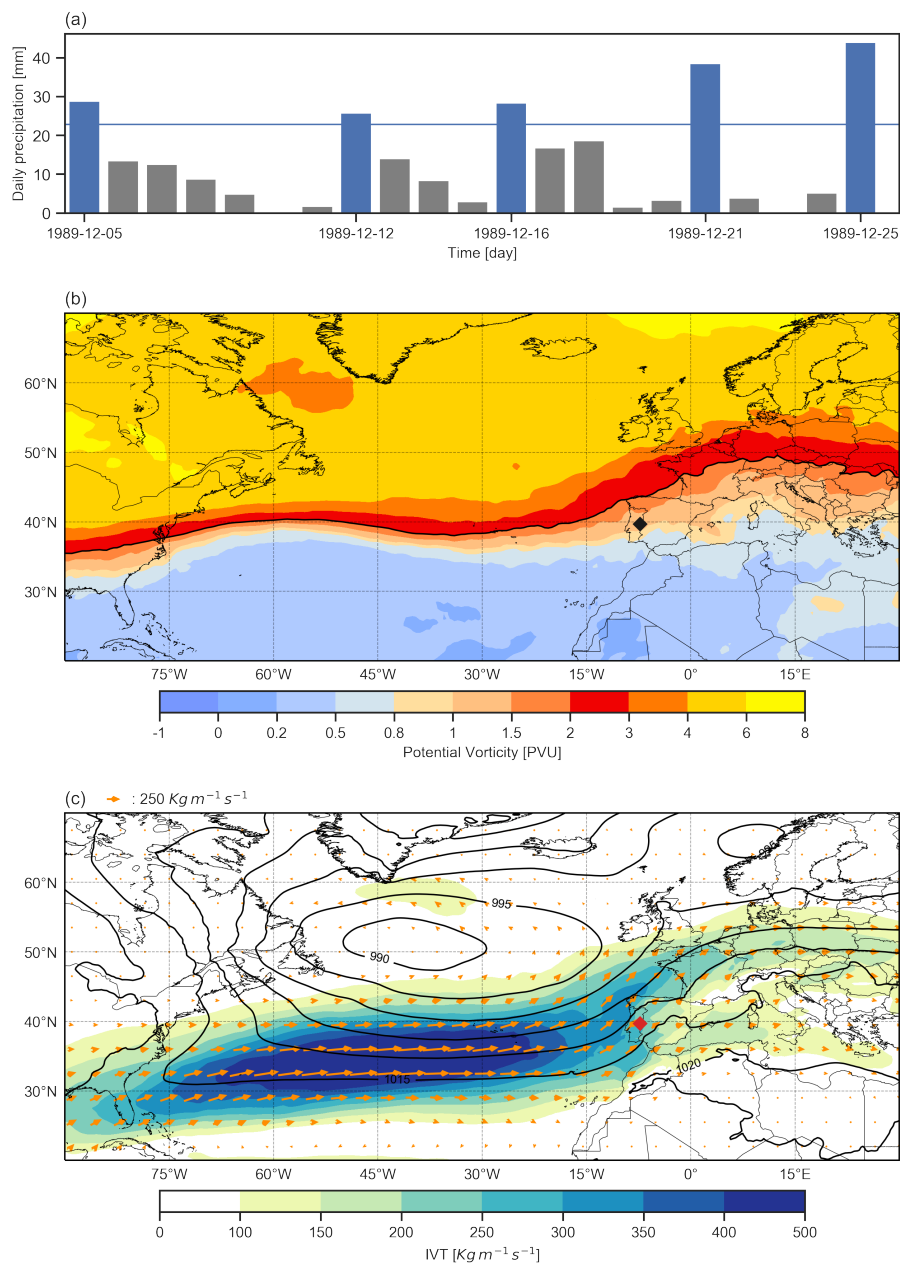


**Figure 11.** Example of a sub-seasonal clustering episode identified with our procedure for catchment 2060654920 of HydroBASINS. (a) Daily precipitation with extreme precipitation events marked by blue bars. The horizontal blue line represents the 99p of the catchment area daily precipitation distribution. (b) Potential Vorticity composite in PVU on the 320-K isentropic level (color shading) and dynamical tropopause identified by the 2 PVU contour (black line). (c) Integrated Vapor Transport composite magnitude (shading) and field in  $\text{Kg m}^{-1} \text{s}^{-1}$  (arrows), and SLP composite in hPa (black contours). The black and red markers indicate the catchment location in panel (b), and (c) respectively. Both composites were calculated as the mean of the ERA5 6-hourly fields during the episode.



*Code and data availability.* ERA5 data are available on the Copernicus Climate Change Service (C3S) Climate Data Store: <https://cds.climate.copernicus.eu/cdsapp#!/dataset/reanalysis-era5-single-levels?tab=form>.

HydroBASINS data are available on the HydroSHEDS website: <https://www.hydrosheds.org/downloads>.

- 315 The complete code used to identify the clustering episodes, compute the metrics and generate all the figures is available on the following github page: [https://github.com/jekopp-git/subseasonal\\_clustering](https://github.com/jekopp-git/subseasonal_clustering) Datasets created in this study are available from FAIR-aligned repository in the in-text data citation Kopp (2021)

### **Appendix A: Data of Fig. 9a and 9b**



**Table A1.** Descriptive statistics of the  $S_r$  distributions for all parameter combinations. The measures are, from top to bottom: the mean value, the standard deviation, the minimum value, the first quartile, the median value, the third quartile and the maximum value.

Measure	r2t99w14	r2t99w21	r2t99w28	r1t99w14	r1t99w21	r1t99w28	r2t98w14	r2t98w21	r2t98w28	r1t98w14	r1t98w21	r1t98w28
Mean	0.78	0.78	0.78	0.79	0.79	0.79	0.78	0.81	0.82	0.80	0.82	0.83
Std	0.06	0.07	0.07	0.06	0.07	0.07	0.05	0.05	0.05	0.05	0.05	0.05
Min	0.42	0.38	0.32	0.44	0.37	0.31	0.53	0.53	0.55	0.57	0.54	0.53
Q1	0.75	0.74	0.74	0.75	0.75	0.75	0.75	0.78	0.79	0.77	0.79	0.80
Median	0.79	0.79	0.79	0.80	0.80	0.80	0.79	0.81	0.82	0.81	0.82	0.84
Q3	0.83	0.83	0.84	0.84	0.84	0.84	0.82	0.84	0.85	0.84	0.85	0.86
Max	0.95	0.93	0.96	0.95	0.95	0.97	0.93	0.93	0.94	0.94	0.94	0.95



**Table A2.** Descriptive statistics of the distributions of the difference between the initial parameter combination ( $r = 2$  days,  $t = 99p$ ,  $w = 21$  days) and the other combinations. The measures are the same as in Table A1.

Measure	r2t99w14	r2t99w28	r1t99w14	r1t99w21	r1t99w28	r2t98w14	r2t98w21	r2t98w28	r1t98w14	r1t98w21	r1t98w28
Mean	0.00	0.00	0.01	0.01	0.01	0.00	0.03	0.04	0.02	0.04	0.05
Std	0.04	0.04	0.04	0.02	0.04	0.07	0.06	0.06	0.07	0.06	0.06
Min	-0.16	-0.14	-0.16	-0.05	-0.16	-0.27	-0.21	-0.19	-0.26	-0.20	-0.17
Q1	-0.03	-0.02	-0.02	0.00	-0.01	-0.04	-0.01	0.00	-0.02	0.00	0.01
Median	0.00	0.00	0.01	0.00	0.01	0.00	0.03	0.04	0.02	0.04	0.05
Q3	0.03	0.03	0.04	0.02	0.03	0.05	0.06	0.08	0.07	0.08	0.09
Max	0.23	0.16	0.20	0.13	0.18	0.35	0.35	0.35	0.38	0.34	0.34



*Author contributions.* JK developed the count-based procedure and metrics, carried out the data analyses and wrote the paper. OM, PR and  
320 SMA developed the concept for the analysis, provided advice on the methodology and on data analysis, discussed the results and contributed  
to the writing. YB supported the statistical analyses and contributed to the writing.

*Competing interests.* The authors declare that they have no conflict of interest.

*Acknowledgements.* The authors thank Andrey Martynov for preparing the ERA5 reanalysis data set and Alexandre Tuel for feedback on  
the draft.





## 325 References

- Barton, Y., Giannakaki, P., von Waldow, H., Chevalier, C., Pfahl, S., and Martius, O.: Clustering of regional-scale extreme precipitation events in southern Switzerland, *Monthly Weather Review*, 144, 347–369, <https://doi.org/10.1175/MWR-D-15-0205.1>, 2016.
- Bevacqua, E., Zappa, G., and Shepherd, T. G.: Shorter cyclone clusters modulate changes in European wintertime precipitation extremes, *Environmental Research Letters*, 15, 124 005, <https://doi.org/10.1088/1748-9326/abbde7>, 2020.
- 330 Coles, S.: *An Introduction to Statistical Modeling of Extreme Values*, vol. 208, Springer, London, 2001.
- Cox, D. R. and Isham, V.: *Point processes*, vol. 12, Chapman & Hall, New York, 1980.
- Dacre, H. F. and Pinto, J. G.: Serial clustering of extratropical cyclones: a review of where, when and why it occurs, *npj Climate and Atmospheric Science*, 3, 1–10, <https://doi.org/10.1038/s41612-020-00152-9>, 2020.
- Dixon, P. M.: Ripley's K Function, *Wiley StatsRef: Statistics Reference Online*, 3, 1796–1803, <https://doi.org/10.1002/9781118445112.stat07751>, 2002.
- 335 European Environment Agency: Economic losses from climate-related extremes in Europe, <https://www.eea.europa.eu/data-and-maps/indicators/direct-losses-from-weather-disasters-4/assessment>, accessed: 26 January 2021, 2020.
- Ferro, C. A. T. and Segers, J.: Inference for clusters of extreme values, *Journal of the Royal Statistical Society: Series B (Statistical Methodology)*, 65, 545–556, <https://doi.org/10.1111/1467-9868.00401>, 2003.
- 340 Fukutome, S., Liniger, M. A., and Süveges, M.: Automatic threshold and run parameter selection: a climatology for extreme hourly precipitation in Switzerland, *Theoretical and Applied Climatology*, 120, 403–416, <https://doi.org/10.1007/s00704-014-1180-5>, 2015.
- Guo, Y., Wu, Y., Wen, B., Huang, W., Ju, K., Gao, Y., and Li, S.: Floods in China, COVID-19, and climate change, *The Lancet Planetary Health*, 4, e443–e444, [https://doi.org/10.1016/S2542-5196\(20\)30203-5](https://doi.org/10.1016/S2542-5196(20)30203-5), 2020.
- Henrion, R. and Seeger, A.: On properties of different notions of centers for convex cones, *Set-Valued and Variational Analysis*, 18, 205–231, <https://doi.org/10.1007/s11228-009-0131-2>, 2010.
- 345 Hersbach, H., Bell, B., Berrisford, P., Hirahara, S., Horányi, A., Muñoz-Sabater, J., Nicolas, J., Peubey, C., Radu, R., Schepers, D., Simmons, A., Soci, C., Abdalla, S., Abellan, X., Balsamo, G., Bechtold, P., Biavati, G., Bidlot, J., Bonavita, M., De Chiara, G., Dahlgren, P., Dee, D., Diamantakis, M., Dragani, R., Flemming, J., Forbes, R., Fuentes, M., Geer, A., Haimberger, L., Healy, S., Hogan, R. J., Hólm, E., Janisková, M., Keeley, S., Laloyaux, P., Lopez, P., Lupu, C., Radnoti, G., de Rosnay, P., Rozum, I., Vamborg, F., Vil-  
350 laume, S., and Thépaut, J.-N.: The ERA5 global reanalysis, *Quarterly Journal of the Royal Meteorological Society*, 146, 1999–2049, <https://doi.org/10.1002/qj.3803>, 2020.
- IPCC: *Climate Change 2014: Impacts, Adaptation, and Vulnerability. Part A: Global and Sectoral Aspects. Contribution of Working Group II to the Fifth Assessment Report of the Intergovernmental Panel on Climate Change* [Field, C.B., V.R. Barros, D.J. Dokken, K.J. Mach, M.D. Mastrandrea, T.E. Bilir, M. Chatterjee, K.L. Ebi, Y.O. Estrada, R.C. Genova, B. Girma, E.S. Kissel, A.N. Levy, S. MacCracken, P.R. Mastrandrea, and L.L. White (eds.)], <https://www.ipcc.ch/report/ar5/wg2/>, 2014.
- 355 Jordahl, K., den Bossche, J. V., Wasserman, J., McBride, J., Gerard, J., Fleischmann, M., Tratner, J., Perry, M., Farmer, C., Hjelle, G. A., Gillies, S., Cochran, M., Bartos, M., Culbertson, L., Eubank, N., maxalbert, Rey, S., Bilogur, A., Arribas-Bel, D., Ren, C., Wilson, J., Journois, M., Wolf, L. J., Wasser, L., Ömer Özak, YuichiNotoya, Leblanc, F., Filipe, Holdgraf, C., and Greenhall, A.: *geopandas/geopandas: v0.6.0*, <https://doi.org/10.5281/zenodo.3463125>, 2019.
- 360 Kopp, J.: Dataset for "A novel method to identify sub- seasonal clustering episodes of extreme precipitation events and their contributions to large accumulation periods", Zenodo [data set], <https://doi.org/10.5281/zenodo.4481893>, 2021.



- Lackmann, G.: Midlatitude Synoptic Meteorology: Dynamics, Analysis, and Forecasting, American Meteorological Society, Boston, MA, 2011.
- Lau, W. K. M. and Kim, K.-M.: The 2010 Pakistan Flood and Russian Heat Wave: Teleconnection of Hydrometeorological Extremes, *Journal of Hydrometeorology*, 13, 392–403, <https://doi.org/10.1175/JHM-D-11-016.1>, 2012.
- 365 Lehner, B. and Grill, G.: Global river hydrography and network routing: baseline data and new approaches to study the world's large river systems, *Hydrological Processes*, 27, 2171–2186, 2013.
- Lenggenhager, S. and Martius, O.: Atmospheric blocks modulate the odds of heavy precipitation events in Europe, *Climate Dynamics*, 53, 4155–4171, <https://doi.org/10.1007/s00382-019-04779-0>, 2019.
- 370 Mailier, P. J., Stephenson, D. B., Ferro, C. A. T., Hodges, K. I., Mailier, P. J., Stephenson, D. B., Ferro, C. A. T., and Hodges, K. I.: Serial Clustering of Extratropical Cyclones, *Monthly Weather Review*, 134, 2224–2240, <https://doi.org/10.1175/MWR3160.1>, 2006.
- Martius, O., Sodemann, H., Joos, H., Pfahl, S., Winschall, A., Croci-Maspoli, M., Graf, M., Madonna, E., Mueller, B., Schemm, S., Sedláček, J., Sprenger, M., and Wernli, H.: The role of upper-level dynamics and surface processes for the Pakistan flood of July 2010, *Quarterly Journal of the Royal Meteorological Society*, 139, 1780–1797, <https://doi.org/https://doi.org/10.1002/qj.2082>, 2013.
- 375 Pinto, J. G., Bellenbaum, N., Karremann, M. K., and Della-Marta, P. M.: Serial clustering of extratropical cyclones over the North Atlantic and Europe under recent and future climate conditions, *Journal of Geophysical Research: Atmospheres*, 118, 12,476–12,485, <https://doi.org/10.1002/2013JD020564>, 2013.
- Priestley, M. D., Pinto, J. G., Dacre, H. F., and Shaffrey, L. C.: The role of cyclone clustering during the stormy winter of 2013/2014, *Weather*, 72, 187–192, <https://doi.org/10.1002/wea.3025>, 2017.
- 380 Priestley, M. D. K., Dacre, H. F., Shaffrey, L. C., Hodges, K. I., and Pinto, J. G.: The role of serial European windstorm clustering for extreme seasonal losses as determined from multi-centennial simulations of high-resolution global climate model data, *Natural Hazards and Earth System Sciences*, 18, 2991–3006, <https://doi.org/10.5194/nhess-18-2991-2018>, 2018.
- Raymond, C., Horton, R. M., Zscheischler, J., Martius, O., AghaKouchak, A., Balch, J., Bowen, S. G., Camargo, S. J., Hess, J., Kornhuber, K., Oppenheimer, M., Ruane, A. C., Wahl, T., and White, K.: Understanding and managing connected extreme events, *Nature Climate Change*, 10, 611–621, <https://doi.org/10.1038/s41558-020-0790-4>, 2020.
- 385 Ripley, B. D.: *Spatial Statistics*, John Wiley & Sons, Hoboken, NJ, 1981.
- Rivoire, P., Martius, O., and Naveau, P.: A comparison of moderate and extreme ERA-5 daily precipitation with two observational data sets, *Earth and Space Science Open Archive*, p. 22, <https://doi.org/10.1002/essoar.10505726.1>, 18 January 2021.
- Sitarz, S.: The medal points' incenter for rankings in sport, *Applied Mathematics Letters*, 26, 408–412, <https://doi.org/10.1016/j.aml.2012.10.014>, 2013.
- 390 Smith, J. A. and Karr, A. F.: Flood Frequency Analysis Using the Cox Regression Model, *Water Resources Research*, 22, 890–896, <https://doi.org/10.1029/WR022i006p00890>, 1986.
- Stephenson, A. G.: evd: Extreme Value Distributions, *R News*, 2, 0, <https://CRAN.R-project.org/doc/Rnews/>, 2002.
- Villarini, G., Smith, J. A., Baeck, M. L., Vitolo, R., Stephenson, D. B., and Krajewski, W. F.: On the frequency of heavy rainfall for the Midwest of the United States, *Journal of Hydrology*, 400, 103–120, <https://doi.org/10.1016/j.jhydrol.2011.01.027>, 2011.
- 395 Villarini, G., Smith, J. A., Serinaldi, F., Ntelekos, A. A., and Schwarz, U.: Analyses of extreme flooding in Austria over the period 1951–2006, *International Journal of Climatology*, 32, 1178–1192, <https://doi.org/10.1002/joc.2331>, 2012.
- Villarini, G., Smith, J. A., Vitolo, R., and Stephenson, D. B.: On the temporal clustering of US floods and its relationship to climate teleconnection patterns, *International Journal of Climatology*, 33, 629–640, <https://doi.org/10.1002/joc.3458>, 2013.



- 400 Vitolo, R., Stephenson, D. B., Cook, I. M., and Mitchell-Wallace, K.: Serial clustering of intense European storms, *Meteorologische Zeitschrift*, 18, 411–424, <https://doi.org/10.1127/0941-2948/2009/0393>, 2009.
- Webster, P. J., Toma, V. E., and Kim, H.-M.: Were the 2010 Pakistan floods predictable?, *Geophysical Research Letters*, 38, <https://doi.org/https://doi.org/10.1029/2010GL046346>, 2011.
- Wilks, D. S.: *Statistical Methods in the Atmospheric Sciences*, vol. 100, Academic press, Oxford; Waltham, MA, 2011.
- 405 Yang, Z. and Villarini, G.: Examining the capability of reanalyses in capturing the temporal clustering of heavy precipitation across Europe, *Climate Dynamics*, 53, 1845–1857, <https://doi.org/10.1007/s00382-019-04742-z>, 2019.
- Zscheischler, J., Martius, O., Westra, S., Bevacqua, E., Raymond, C., Horton, R. M., van den Hurk, B., AghaKouchak, A., Jézéquel, A., Mahecha, M. D., Maraun, D., Ramos, A. M., Ridder, N. N., Thiery, W., and Vignotto, E.: A typology of compound weather and climate events, *Nature Reviews Earth & Environment*, pp. 1–15, <https://doi.org/10.1038/s43017-020-0060-z>, 2020.